Gaussian accelerated molecular dynamics with the weighted ensemble method: a hybrid method improves thermodynamic and kinetic sampling

Surl-Hee Ahn,*,†,¶ Anupam A. Ojha,†,¶ Rommie E. Amaro,† and J. Andrew McCammon†,‡

†*Department of Chemistry, University of California San Diego, La Jolla, CA, USA*

‡*Department of Pharmacology, University of California San Diego, La Jolla, CA, USA*

¶*These authors have contributed equally.*

E-mail: s3ahn@ucsd.edu

Abstract

Gaussian accelerated molecular dynamics (GaMD) is a well-established enhanced sampling method for molecular dynamics (MD) simulations that effectively samples the potential energy landscape of the system by adding a boost potential, which smoothens the surface and lowers energy barriers between states. GaMD is unable to give time-dependent properties such as kinetics directly. On the other hand, the weighted ensemble (WE) method can efficiently sample transitions between states with its many weighted trajectories, which directly yield rates and pathways. However, the performance of WE (i.e., convergence and efficiency) depends heavily on its initial conditions or initial sampling of the potential energy landscape. Hence, we have developed a hybrid method that combines the two methods, wherein GaMD is first used to sample the potential energy landscape of the system, and WE is subsequently used to further sample the potential energy landscape and kinetic properties of interest. We show

that the hybrid method can sample both thermodynamic and kinetic properties more accurately and quickly compared to using either method alone.

1 Introduction

Molecular dynamics (MD) simulations are becoming quintessential tools in many fields, including biology, chemistry, materials science, chemical and biological engineering, and medicine. An increasing number of researchers have used MD simulations to uncover mechanisms of their biological system of interest in atomistic detail. Applications of MD simulations range from studying protein folding, protein-protein or protein-ligand interactions to computer-aided drug design (virtual screening and ligand docking). However, MD simulations are not without their challenges. MD simulations have to be run using femtosecond time steps due to being limited by the fastest motions in the system. In contrast, biological processes of interest are on the order of microseconds or longer. Additionally, systems often get "stuck" in metastable states and do not change conformations for an extended period. Hence, MD simulations can be computationally costly when attempting to observe rare events, which is often the case of interest.

Fortunately, researchers have developed several "enhanced sampling methods" to overcome this timescale gap between MD simulations and biological processes. Many enhanced sampling methods work by adding a biasing potential to force the system away from metastable states. These include but are not limited to Gaussian accelerated dynamics (GaMD),[1–4] metadynamics,[5–9] umbrella sampling,[10–13] and adaptive biasing force (ABF).[14–18] Among these, GaMD has the advantage of not requiring any collective variables (CVs) to steer the simulation. Rather, it allows unrestrained sampling of configuration space. Another similar class of methods changes the system's temperature instead to sample states difficult to reach at room temperature, including replica exchange molecular dynamics (REMD) or parallel tempering.[19–23] Although both of these classes of methods are effective at obtain-

ing thermodynamic properties like the free energy landscape of the system, they alter the actual kinetics of the system, preventing them from directly getting kinetic properties from the system. Note that there are methods to derive kinetic properties like rate constants from simulations that used these methods. Still, they need to be obtained either by using Kramers' Rate Theory in the high friction or "overdamping" regime,[24] constructing a master equation,[25,26] or assuming a low residence time in the transition states.[27]

As a result, several path-sampling methods focus on sampling kinetic properties, such as rate constants from the reactant state to the product state, including milestoning,[28–32] forward flux sampling,[33–36] transition interface sampling,[37–40] and others. These methods divide the path space from reactant state to product state into many interfaces and run many short simulations to efficiently obtain rate constants and the free energy landscape of the path space. However, since these methods primarily focus on sampling the path of interest, the rest of the free energy landscape is not extensively sampled.

Suppose a more comprehensive picture of the entire configuration space is needed along with its thermodynamic and kinetic properties. In that case, either one can build a Markov state model (MSM)[41–48] or run the weighted ensemble (WE) method[49–59] on the system of interest. Both methods decompose the configuration space into small volume elements called "macrostates" and run many short simulations to obtain good statistics. The macrostate construction with feature selection or appropriate CVs and setting parameters such as lag time or simulation time τ differ between the two methods. This difference is due to MSMs requiring Markovian property to hold and being constructed with MD trajectories of the system. In contrast, WE starts sampling the system after the macrostate construction, and parameters such as the simulation time τ are set *a priori*. Both methods have proven to be useful in uncovering insights into the mechanisms of important biophysical systems.[60–77] However, both require a sufficient sampling of the configuration space either by having many long MD trajectories or by having many initial configurations to get accurate results quickly.

As a result, we have developed a hybrid enhanced sampling method that combines GaMD

and WE called GaMD-WE. There also exist hybrid methods that combine REMD and GaMD[78,79] and well-tempered metadynamics and GaMD,[80] but both aim to improve sampling of thermodynamic properties. In contrast, GaMD-WE aims to enhance sampling of both thermodynamic and kinetic properties. In GaMD-WE, GaMD is initially run to sample the free energy landscape efficiently with its harmonic boost potentials. Then, after reweighting is performed to recover the original free energy landscape, WE is run with many initial configurations produced from the GaMD run. This way, the two methods complement each other and reduce each other's limitations. This paper will introduce both methods, the hybrid method, and the results that demonstrate the hybrid method's power to obtain thermodynamic and kinetic properties more accurately and more quickly than one method by itself.

2 Methods

2.1 Gaussian accelerated molecular dynamics

Gaussian accelerated molecular dynamics (GaMD) is an enhanced sampling method for MD simulations that can efficiently sample thermodynamic properties such as the free energy landscape of the system. When the system potential $V(\mathbf{r})$, where $\mathbf{r}$ denotes the position vector of an N-atom system, is lower than a threshold energy E, GaMD fills the energy wells by adding a harmonic boost potential $\Delta V(\mathbf{r})$, i.e.,

$$\Delta V(\mathbf{r}) = \frac{1}{2} k \left(E - V(\mathbf{r})\right)^2, \tag{1}$$

where k denotes the harmonic force constant. If $V(\mathbf{r}) \geq E$, then no boost potential is added. There are several criteria that the boost potential $\Delta V(\mathbf{r})$ needs to satisfy for GaMD to work, and readers can refer to the original GaMD paper[1] for specific details about the boost potential $\Delta V(\mathbf{r})$ and the harmonic force constant k.

If the anharmonicity of the harmonic boost potential $\Delta V(\mathbf{r})$ is small, then $\Delta V(\mathbf{r})$ follows a near Gaussian distribution and the cumulant expansion to the second order can be used to approximate the exponential average term $\langle e^{\beta \Delta V(\mathbf{r})} \rangle$, where β denotes the thermodynamic beta or $1/k_B T$. This exponential average term $\langle e^{\beta \Delta V(\mathbf{r})} \rangle$ is needed to reweight and recover the original free energy landscape from GaMD. Readers can refer to the original GaMD paper[1] for specific details about energetic reweighting with cumulant expansion to the second order.

A significant advantage of GaMD is that CVs, which describe the state of a molecular system, are not needed. Identifying the appropriate CVs for a particular system is still an active area of research and can be difficult for new or unfamiliar systems.[81–83] In contrast, metadynamics requires CVs to be chosen *a priori*, which similarly fills energy wells with repulsive Gaussian potentials. However, metadynamics does not suffer from having unconverged high energy regions like GaMD since metadynamics recovers the original free energy landscape as the opposite sum of all Gaussians. Nonetheless, GaMD is one of the few enhanced sampling methods that do not require tuning of many parameters and can be easily applied to various systems. Additionally, GaMD is fully implemented in Amber[84] (starting from Amber16) and NAMD[85] (starting from 2.13),[2] which makes it easier for users to use the method.

2.2 Weighted ensemble method

The weighted ensemble (WE) method is another enhanced sampling method for MD simulations that runs many short simulations instead of one long simulation to sample thermodynamic and kinetic properties efficiently. These short simulations or "walkers" carry probabilities or "weights" that evolve throughout the simulation via "resampling," a statistical procedure to maintain a number of these short simulations at visited regions of the configuration space. More details can be found in the original WE paper,[49] in a review article,[50] and in the Weighted Ensemble Simulation Toolkit with Parallelization and Analysis (WESTPA) papers,[86,87] but the general scheme is as follows.

1. The following parameters are chosen *a priori* for the WE simulation: CVs, simulation time τ for walkers, partitioning of macrostates (small volume elements of the configuration space), and target number of walkers per macrostate n_w. If there is only one initial state, then there will be n_w walkers, each with a weight of $1/n_w$. Otherwise, there will be multiple n_w walkers, each with an appropriate weight that sums up to 1 for the entire system.

2. Walkers are run for τ amount of time and binned to appropriate macrostates depending on their CV values.

3. Walkers go through "resampling," i.e., merged or replicated in a statistically correct way so that the target number of walkers per macrostate n_w is maintained for each macrostate. Each walker ends up with a weight between P_i/n_w and $2P_i/n_w$ where P_i denotes the sum of the weights in macrostate i.

4. Steps 2 and 3 are repeated until desired convergence is reached.

With resampling, the walkers are maintained in each visited macrostate regardless of its energy barrier height. Computational cost is also curtailed since walkers are merged in oversampled, low energy regions and replicated in rare, high energy regions. Since no statistical bias is added to the system, one can directly obtain both thermodynamic and kinetic properties of the system from the evolution of walkers' weights in each macrostate.

Although several parameters need to be chosen *a priori* as stated in Step 1, simulation time τ can be selected without having to worry about fulfilling the Markovian property, a requirement that other enhanced sampling methods have such as Markov State Models (MSMs) and milestoning. The simulation time τ should be chosen to be short enough so that WE does not inadvertently miss transitions.[53,74,88] However, since many macrostates have to reach convergence to extract correct thermodynamic and kinetic properties of the system, WE can be computationally costly if the initial states are not close to steady-state.

2.3 Gaussian accelerated molecular dynamics-weighted ensemble method

The hybrid Gaussian accelerated molecular dynamics-weighted ensemble (GaMD-WE) method aims to combine strengths and mitigate weaknesses of both methods. By initially running GaMD to sample the free energy landscape of the system, one can obtain a well-sampled initial state distribution for WE. Then with WE, one can get a more refined free energy landscape closer to steady-state and sample kinetic properties such as rate constants from one state to another state. We show that the hybrid method is significantly more effective than running a conventional WE to sample thermodynamic and kinetic properties within the same amount of simulation time in the subsequent Results section.

We have developed a GaMD-WE package for users to run GaMD and prepare initial states for WE, specifically for the Weighted Ensemble Simulation Toolkit with Parallelization and Analysis (WESTPA).[86,87] The current package is not fully integrated with WESTPA, i.e., user needs to use the GaMD-WE package for the GaMD portion and run a WESTPA simulation separately for the WE portion using initial states from the GaMD-WE package, but we plan to make it fully integrated in the future. The GaMD-WE package is fully customizable, i.e., the desired force fields, water models, and others can be added, and it follows a series of scripts as the following.

1. System is prepared for simulation after the Protein Data Bank (PDB) structure is downloaded from the PDB server. Appropriate force field parameters are added followed by system solvation.

2. Solvated system is then minimized, heated, and equilibrated using the OpenMM[89] simulation engine. Directories are created for the subsequent GaMD simulations.

3. Six GaMD simulations are run using the Amber[84] simulation engine for varying degrees of potential boosts, i.e., dihedral potential boost (upper and lower bound), total

potential boost (upper and lower bound), and dual (dihedral + total) potential boost (upper and lower bound), for the desired amount of simulation time.

4. Simulation data is then extracted from the output log files for each of the six GaMD simulations. Reweighting is then performed with several reweighting methods, i.e., cumulant expansion to the first order, second order, and third order, to recover the original free energy landscape. Then with the desired target number of walkers per macrostate n_w, initial structures/configurations for WE are saved with appropriate weights from the binning probabilities.

5. Initial structures for WE are minimized in two steps (Step 1: Heavy atoms C_α, N, C, O of the protein are minimized, Step 2: Entire system including solvent is minimized) so that none of them "crash" during WE. User can set the minimization steps.

6. WE simulation directory is created with proper initial structures. Number of initial structures can be compared among the six simulation outputs (see Supplementary Information). GaMD simulation that yielded the largest number of initial structures can be subsequently used for WE simulation since that would indicate the greatest coverage of the free energy landscape.

In the subsequent Results section, we show that GaMD has greater coverage of the free energy landscape and closer to steady-state probabilities compared to WE within the same simulation time. Even if WE has a similar amount of coverage of the free energy landscape compared to GaMD for some systems, GaMD has an advantage over WE with reweighting since appropriate probabilities or weights can be recovered from the added biasing potentials. In contrast, since WE does not add any statistical bias to the system, the system needs to evolve naturally or reach convergence to appropriate probabilities or weights, which in most cases would take longer than adding a biasing potential to the system.

3 Results

We have tested our hybrid method on two systems: alanine dipeptide in explicit solvent and chignolin in implicit solvent. We show how GaMD-WE outperforms either method in obtaining thermodynamic and kinetic properties. To further illustrate that GaMD surpasses WE in getting the free energy landscape, we show the free energy landscapes of bovine pancreatic trypsin inhibitor (BPTI) in explicit solvent obtained from the two methods. Amber ff14SB force field parameters[90] were used for all three systems. Simulations were run under the canonical ensemble, and the temperature T was set to 300 K for all three systems.

Three simulations were run for each system using GaMD-WE and WE, and average of the three is shown as the final result for all systems. Error bars for WE and GaMD-WE rate constants represent 95% confidence intervals (i.e., $1.96 \times \frac{\sigma}{\sqrt{3}}$ where σ denotes standard deviation). Each point in WE and GaMD-WE rate constant graph was calculated cumulatively in 50 iteration blocks.

3.1 Alanine dipeptide

Alanine dipeptide is a 22-atom system that is commonly used as a test system for new methods. Initial structure was obtained from `https://markovmodel.github.io/mdshare/ALA2/`. TIP3P water model[91] was used to solvate the system explicitly. For GaMD-WE, GaMD was run for 50 ns, and WE was run for 11.95 μs so that the total simulation time amounted to 12 μs. Simulation time, τ for WE was set to 10 ps, equal to GaMD's sampling frequency. The target number of walkers per macrostate n_w was set to 4. CVs were set to be the dihedral angles, ϕ and ψ. Macrostates were evenly spaced in intervals of 10° for both ϕ and ψ (ranging from -180° to 180°).

First, we show that GaMD covers the free energy landscape more than WE within the same simulation time. Figures 1a and 1b show the average free energy landscape ($-k_BT \ln P$, where P denotes probability) of alanine dipeptide after 50 ns of GaMD and WE, respec-

tively. The lowest energy state was set to be zero for each of the free energy landscapes. In particular, the GaMD run with the upper bound of the dihedral boost potential yielded the maximum number of initial structures on average as compared to the other five GaMD potential settings (see Supplementary Information). Cumulant expansion to the second order was used for GaMD reweighting. As seen in Figure 1, GaMD can cover the high energy regions such as the left-handed α-helix region α_{L} on the right side, whereas WE cannot sample it within 50 ns of simulation time. This shows that it can be more beneficial to use GaMD instead of WE to sample the free energy landscape, even for this simple system.

Second, we show that GaMD-WE can converge to the correct rate constants faster and more accurately than WE. In particular, rate constants between the three regions of interest shown in Figure 1c were measured over simulation time. α_{R} region was defined to be $-120^\circ \leq \phi \leq 0^\circ$, $-100^\circ \leq \psi \leq 50^\circ$, $\mathrm{P_{II}}$ region was defined to be $-120^\circ \leq \phi \leq 0^\circ$, $100^\circ \leq \psi \leq 180^\circ$, and α_{L} region was defined to be $0^\circ \leq \phi \leq 120^\circ$, $-50^\circ \leq \psi \leq 100^\circ$. Initial structures for the three GaMD-WE runs were from one of the three GaMD runs with an upper bound of dihedral boost potential that yielded the largest number of initial structures. WE and brute force simulations used the same initial structure as the GaMD runs. In addition, since GaMD covered a wider free energy landscape within 50 ns, another set of GaMD-WE simulations was run with equal weights. Although reweighting would give more accurate weights for each region, we wanted to investigate whether there will be any improvements in obtaining kinetics solely from covering more of the free energy landscape with GaMD vs. WE. Figure 2 shows the evolution of rate constants over aggregate simulation time, and Table 1 summarizes the final rate constants for brute force, WE, and GaMD-WE simulations after 12 μs of simulation time. Reference brute force simulation values were obtained from averaging all first passage times from three independent 4 μs runs and performing Bayesian bootstrapping for 95 % confidence intervals.[87] The first 200 ns of simulation time was cut off in the rate constant calculation to eliminate initial structure bias for brute force, WE, and GaMD-WE simulations.

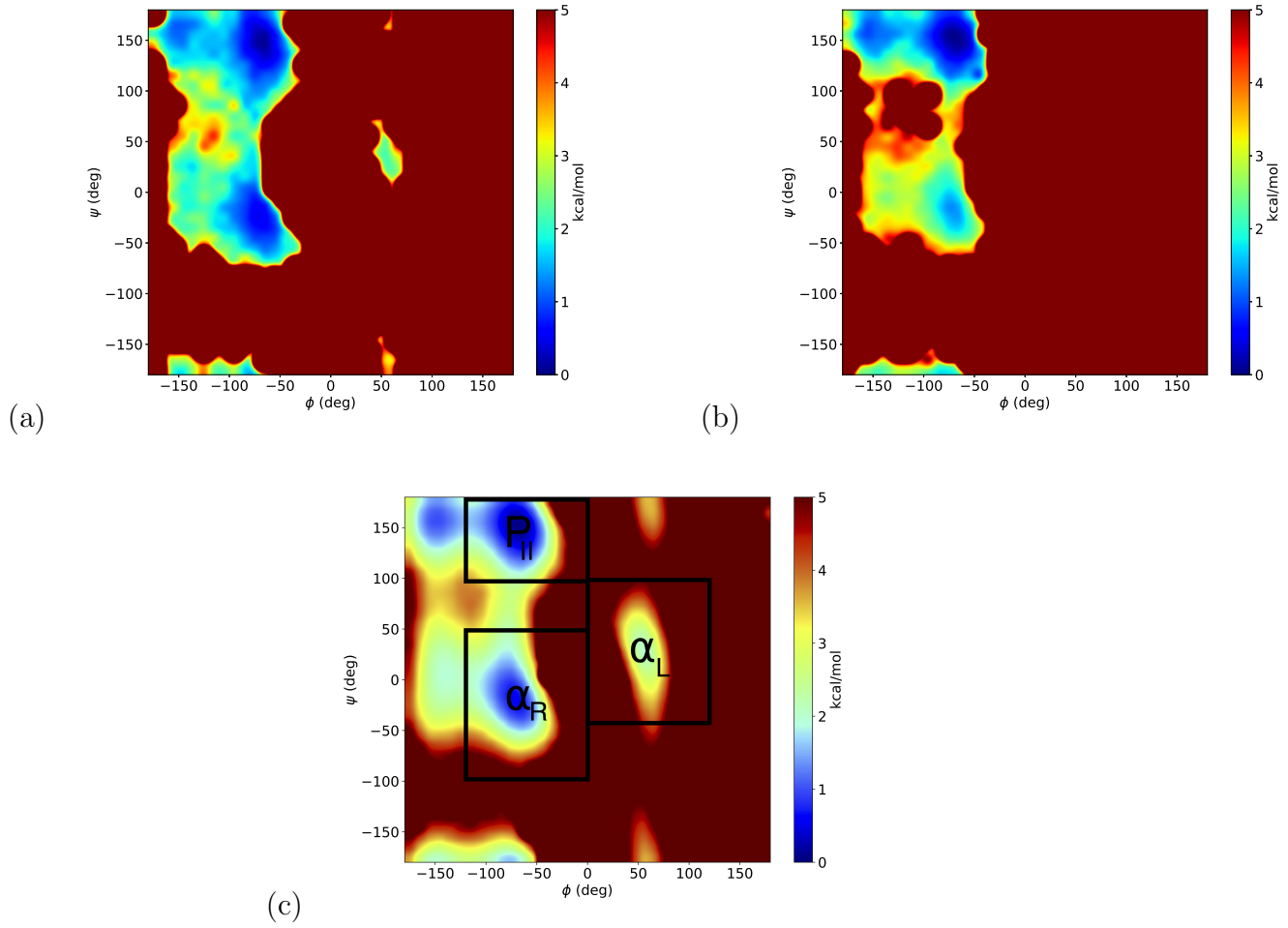

Figure 1: Average free energy landscape ($-k_B T \ln P$, where P denotes probability) of alanine dipeptide after (a) 50 ns of GaMD (with upper bound of dihedral boost potential), and (b) 50 ns of WE, respectively. (c) shows the average free energy landscape obtained after 12 μs of WE (after cutting out the first 200 ns of simulation time to eliminate initial structure bias), with the regions of interest (α_{R}, α_{L}, and $\mathrm{P_{II}}$) marked. The lowest energy state was set to be zero for each free energy landscape.

Figures 2a and 2b show that the convergence is comparable between WE and GaMD-WE for the rate constants between the two central metastable states α_{R} and $\mathrm{P_{II}}$ since both methods covered both regions well. However, GaMD-WE underestimated both rate constants (see Table 1), which WE obtained more accurately. This might be due to GaMD-WE having lower weights than actual for the initial α_{R} and $\mathrm{P_{II}}$ structures, which would slow down the rate of convergence for GaMD-WE. The GaMD-WE simulations with equal weights, on the other hand, had larger error bars than regular GaMD-WE and performed similarly to GaMD-WE.

For the rate constants that involved the higher energy region α_{L}, however, GaMD-WE performed better than WE. Figures 2c and 2e highlight GaMD-WE having the rate constants that go from α_{L} to either primary metastable state α_{R} or $\mathrm{P_{II}}$ converge faster with smaller error bars (see Table 1) compared to WE. GaMD-WE simulations with equal weights, on the other hand, did not perform better than either WE or GaMD-WE. As for the reverse rate constants that go from either primary metastable state α_{R} or $\mathrm{P_{II}}$ to α_{L}, GaMD-WE and WE have comparable performances with GaMD-WE slightly underestimating both rate constants as seen from Figures 2d and 2f and Table 1. GaMD-WE simulations with equal weights performed marginally better than GaMD-WE by underestimating the rate constants lesser. This might be due to having higher weights for the regions of interest than GaMD-WE.

These results indicate that GaMD-WE can obtain kinetics involving higher energy regions like α_{L} faster and more accurately than WE alone. In contrast, WE performs as well as GaMD-WE in getting kinetics involving central metastable states, which both methods can sample sufficiently well. In addition, GaMD-WE needs reweighting to have more accurate weights and have an advantage over WE, i.e., GaMD-WE does not necessarily have an advantage over WE from solely covering more of the free energy landscape within the same simulation time. However, this might not be the case if GaMD had covered a region with a higher energy barrier that is difficult for conventional WE to sample quickly, so this

hypothesis needs to be tested on more complex systems in the future.

Table 1: Alanine dipeptide rate constants (in ns^{-1}) after 12 μs of simulation time. In the brute force simulation column, the first value indicates the average rate constant value, and the second value indicates the 95% confidence interval calculated from Bayesian bootstrapping. For WE and GaMD-WE, the error bars represent 95% confidence intervals calculated from the standard deviation of three independent runs.

	Brute force	WE	GaMD-WE	GaMD-WE with equal weights
$\alpha_R \rightarrow P_{II}$	6.81, [6.71, 6.90]	6.79 ± 0.052	6.54 ± 0.088	6.47 ± 0.12
$P_{II} \rightarrow \alpha_R$	2.97, [2.92, 3.02]	2.96 ± 0.055	2.88 ± 0.035	2.88 ± 0.040
$\alpha_L \rightarrow \alpha_R$	0.30, [0.25, 0.36]	0.38 ± 0.25	0.34 ± 0.087	0.23 ± 0.14
$\alpha_R \rightarrow \alpha_L$	0.0099, [0.0083, 0.012]	0.0083 ± 0.0011	0.0081 ± 0.0021	0.0092 ± 0.0017
$\alpha_L \rightarrow P_{II}$	0.33, [0.27, 0.40]	0.32 ± 0.020	0.33 ± 0.012	0.31 ± 0.019
$P_{II} \rightarrow \alpha_L$	0.0099, [0.0083, 0.012]	0.0085 ± 0.0014	0.0082 ± 0.0020	0.0090 ± 0.0018

3.2 Chignolin

To investigate whether GaMD-WE will be significantly more effective than WE for more complex systems, we tested the two methods on chignolin, a 138-atom system with ten residues (PDB: 1UAO). The modified Generalized Born implicit model with the model II radii[92] was used to solvate the system implicitly. For GaMD-WE, GaMD was run for 500 ns, and WE was run for 39.5 μs so that the total simulation time amounted to 40 μs. Simulation time, τ for WE was set to 20 ps, equal to GaMD's sampling frequency. Target number of walkers per macrostate n_w was set to 4. CVs were set to be the mass-weighted root-mean-square-deviation (RMSD) of C_α atoms from the initial folded state (PDB: 1UAO) and the mass-weighted radius of gyration (R_g) of C_α atoms. Macrostates were evenly spaced in intervals of 0.2 $\mathring{A}$ for both RMSD and R_g (ranging from 0 $\mathring{A}$ to 8 $\mathring{A}$).

Figures 3a and 3b show the average free energy landscape ($-k_B T \ln P$, where P denotes probability) of chignolin after 500 ns of GaMD and WE, respectively. The lowest energy state was set to be zero for each free energy landscape. In particular, the GaMD run with the upper bound of the dihedral boost potential yielded the maximum number of initial structures on average as compared to the other five GaMD potential settings (see

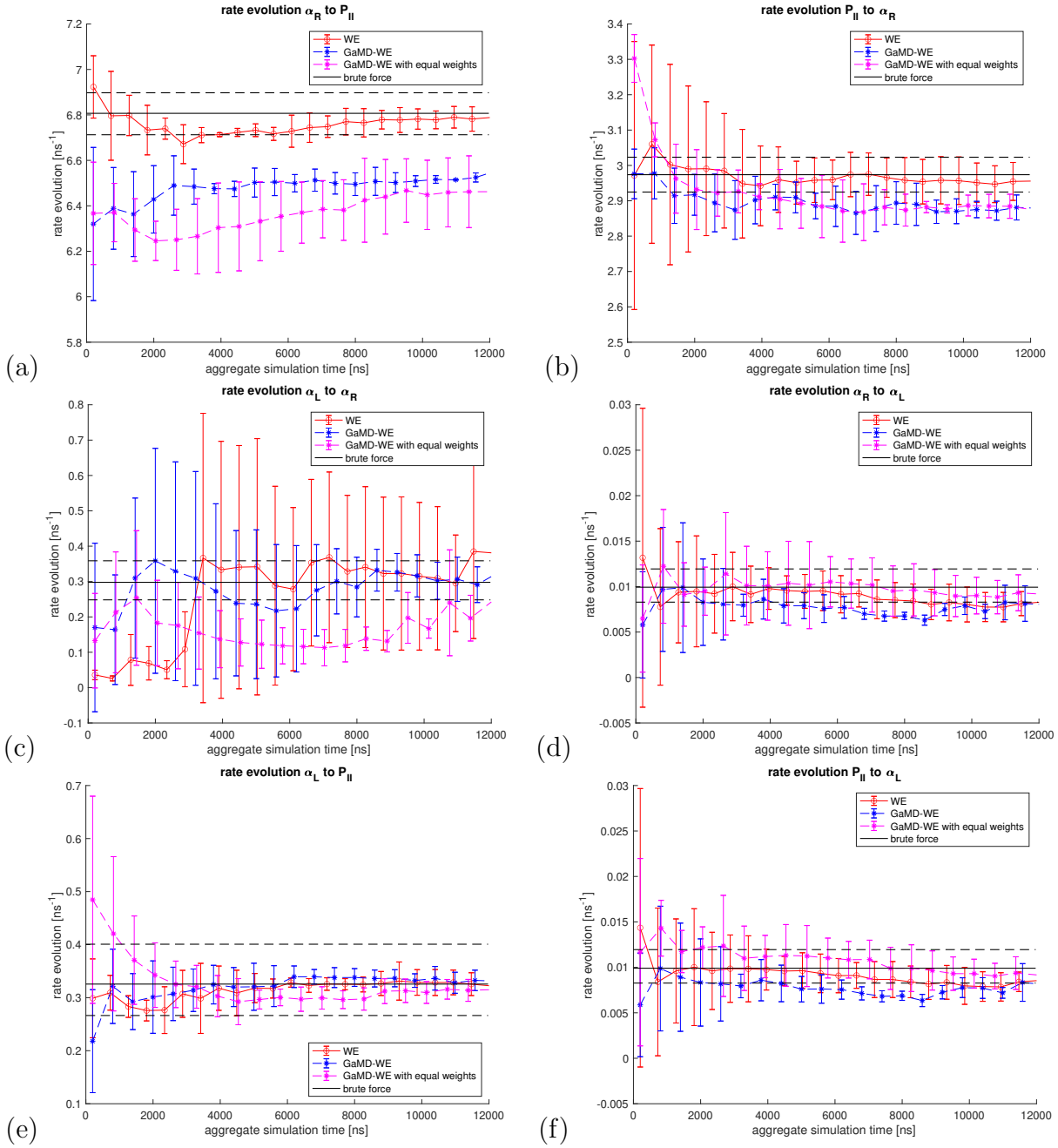

Figure 2: Evolution of rate constants over aggregate simulation time for WE (in red), GaMD-WE (in blue), and GaMD-WE with equal weights (in magenta). The reference brute force values are in black. (a) and (b) show the rate constants between the two major metastable states α_{R} and $\mathrm{P_{II}}$. (c) and (d) show the rate constants between α_{R} and α_{L}, a higher energy region, and (e) and (f) show the rate constants between $\mathrm{P_{II}}$ and α_{L}.

Supplementary Information). Cumulant expansion to the second order was used for GaMD reweighting. Although GaMD and WE have comparable free energy landscape coverage as seen in Figures 3a and 3b, GaMD has probabilities closer to actual values due to reweighting as seen in Figures 3c and 3d. This shows that it can still be more beneficial to use GaMD instead of WE to sample the free energy landscape as GaMD yields a more accurate free energy landscape.

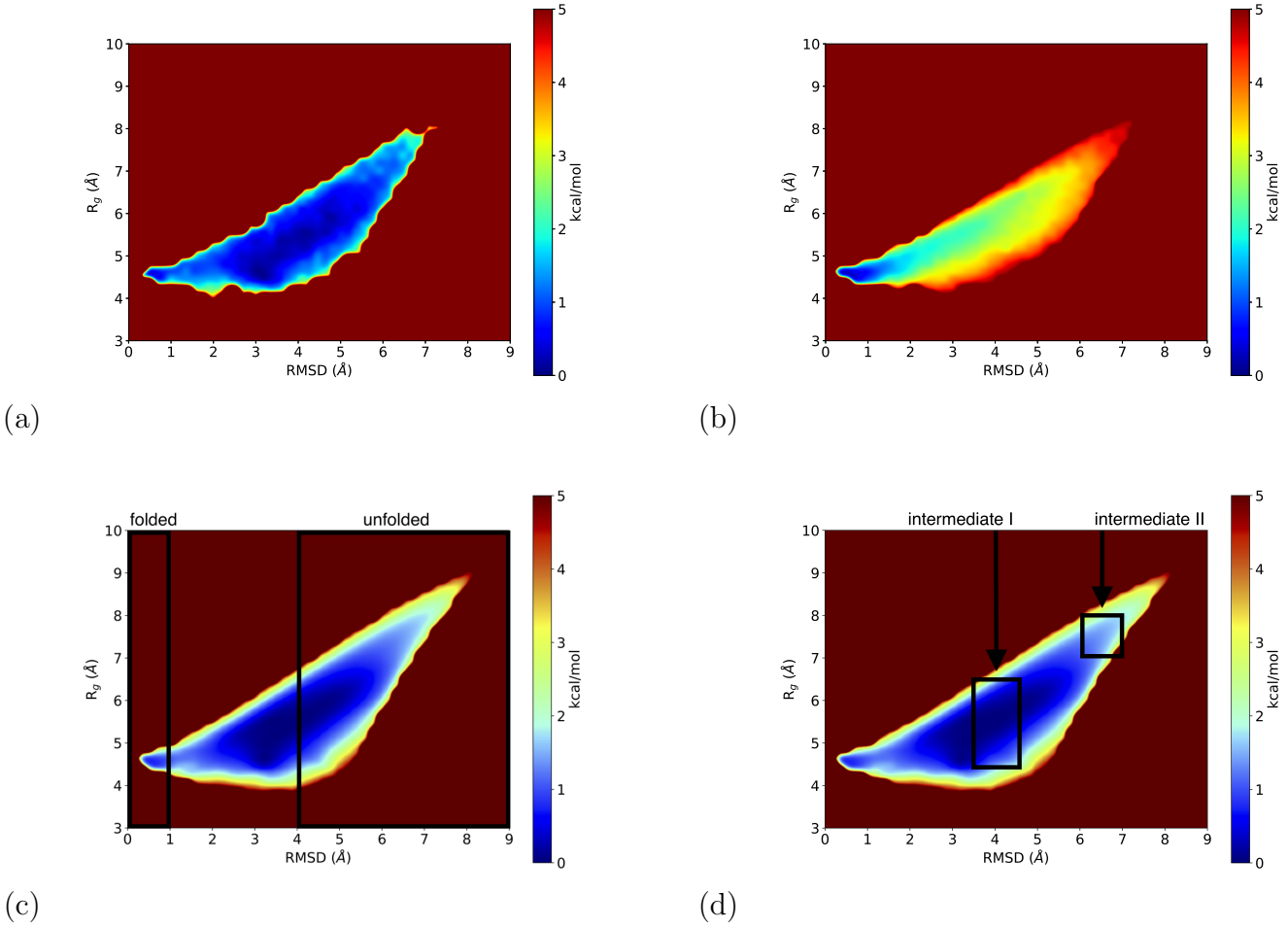

Figure 3: Average free energy landscape ($-k_BT \ln P$, where P denotes probability) of chignolin after (a) 500 ns of GaMD (with upper bound of dihedral boost potential), and (b) 500 ns of WE, respectively. (c) and (d) show the average free energy landscape obtained after 40 μs of WE (after cutting out the first 2 μs of simulation time to eliminate initial structure bias), with the regions of interest marked. The lowest energy state was set to be zero for each free energy landscape.

We also show that GaMD-WE can converge to the correct rate constants faster and more

accurately than WE, more notably than in the alanine dipeptide case. Specifically, rate constants between the four regions of interest shown in Figures 3c and 3d were measured over simulation time. The folded region was defined to be 0.0 $\mathring{A} \leq$ RMSD $\leq$ 1.0 $\mathring{A}$, unfolded region was defined to be 4.0 $\mathring{A} \leq$ RMSD, intermediate I region was defined to be 3.5 $\mathring{A} \leq$ RMSD $\leq$ 4.5 $\mathring{A}$, 4.5 $\mathring{A} \leq R_g \leq$ 6.5 $\mathring{A}$, and the intermediate II region was defined to be 6.0 $\mathring{A} \leq$ RMSD $\leq$ 7.0 $\mathring{A}$, 7.0 $\mathring{A} \leq R_g \leq$ 8.0 $\mathring{A}$. Initial structures for the three GaMD-WE runs were from one of the three GaMD runs with an upper bound of dihedral boost potential that yielded the largest number of initial structures. WE and brute force simulations used the same initial structure as the GaMD runs. Figures 4 and 5 show the evolution of rate constants over aggregate simulation time, and Table 2 summarizes the final rate constants for brute force, WE, and GaMD-WE simulations after 40 μs of simulation time. The reference brute force simulation values were obtained from averaging all first passage times from five independent 8 μs runs and performing Bayesian bootstrapping for 95 % confidence intervals.[87] The first 2 μs of simulation time was cut off in the rate constant calculation to eliminate initial structure bias for brute force, WE, and GaMD-WE simulations.

Figures 4a and 4b show that GaMD-WE is faster than WE at converging to the reference rate constants between the folded and unfolded regions. GaMD-WE is significantly better at obtaining the rate constants from unfolded to folded since GaMD-WE had closer to actual probabilities for the unfolded region with reweighting. Without reweighting, WE takes a significantly longer time to converge to the reference rate constants. Figures 5a, 5b, 5c, and 5d also show similar results that highlight GaMD-WE converging faster to the reference rate constants, especially for rate constants that go from either intermediate I or II region to the folded region. Performance for GaMD-WE is only slightly better than WE in obtaining the rate constants between the intermediate I region and the intermediate II region, however, as seen in Figures 5e and 5f. The two regions are close to each other, making sampling between these two regions and converging to the actual rate constants easier than the other cases. Finally, Table 2 indicates that the only rate constant that WE had within the reference

confidence interval was for the folded → intermediate II rate constant. In contrast, the GaMD-WE had all of the rate constants fall within the confidence intervals except for the intermediate I → intermediate II rate constant. Error bars for GaMD-WE were lower than WE for all rate constants except for the folded → unfolded, unfolded → folded, and folded → intermediate I rate constants. These results indicate that GaMD-WE's performance in obtaining kinetics is significantly better than conventional WE for more complex systems than alanine dipeptide.

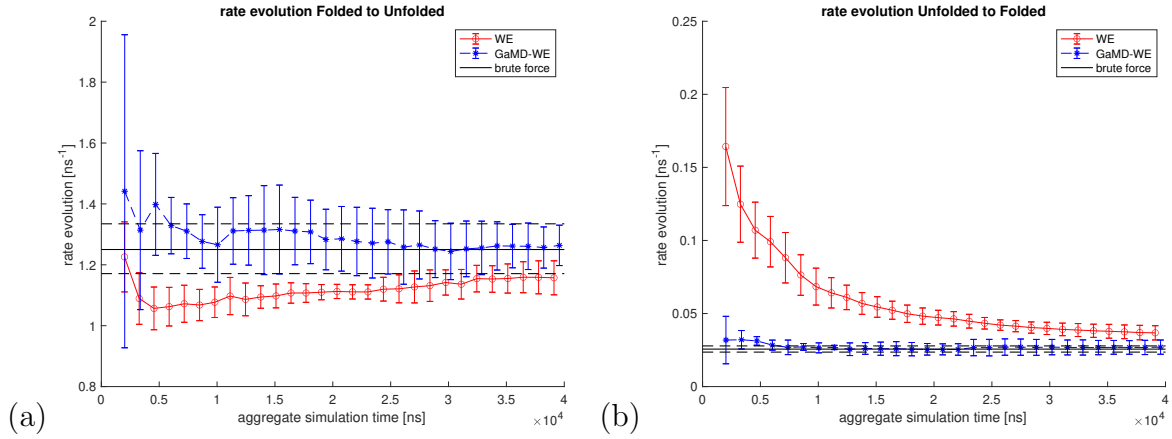

Figure 4: Evolution of rate constants over aggregate simulation time for WE (in red) and GaMD-WE (in blue). The reference brute force values are in black. (a) and (b) show the rate constants between the folded region and the unfolded region.

Table 2: Chignolin rate constants after 40 μs of simulation time. In the brute force simulation column, the first value indicates the average rate constant value, and the second value indicates the 95% confidence interval calculated from Bayesian bootstrapping. For WE and GaMD-WE, the error bars represent 95% confidence intervals calculated from the standard deviation of three independent runs.

	Brute force [ns^{-1}]	WE [ns^{-1}]	GaMD-WE [ns^{-1}]
Folded → Unfolded	1.25, [1.17, 1.33]	1.16 ± 0.056	1.26 ± 0.067
Unfolded → Folded	0.026, [0.024, 0.028]	0.037 ± 0.0049	0.027 ± 0.0049
Folded → Intermediate I	1.41, [1.32, 1.50]	1.26 ± 0.046	1.46 ± 0.089
Intermediate I → Folded	0.028, [0.026, 0.031]	0.041 ± 0.0056	0.029 ± 0.0045
Folded → Intermediate II	0.42, [0.40, 0.45]	0.44 ± 0.040	0.40 ± 0.020
Intermediate II → Folded	0.020, [0.019, 0.022]	0.024 ± 0.0039	0.021 ± 0.0019
Intermediate I → Intermediate II	1.15, [1.13, 1.17]	1.19 ± 0.037	1.20 ± 0.024
Intermediate II → Intermediate I	4.52, [4.46, 4.58]	4.67 ± 0.19	4.52 ± 0.17

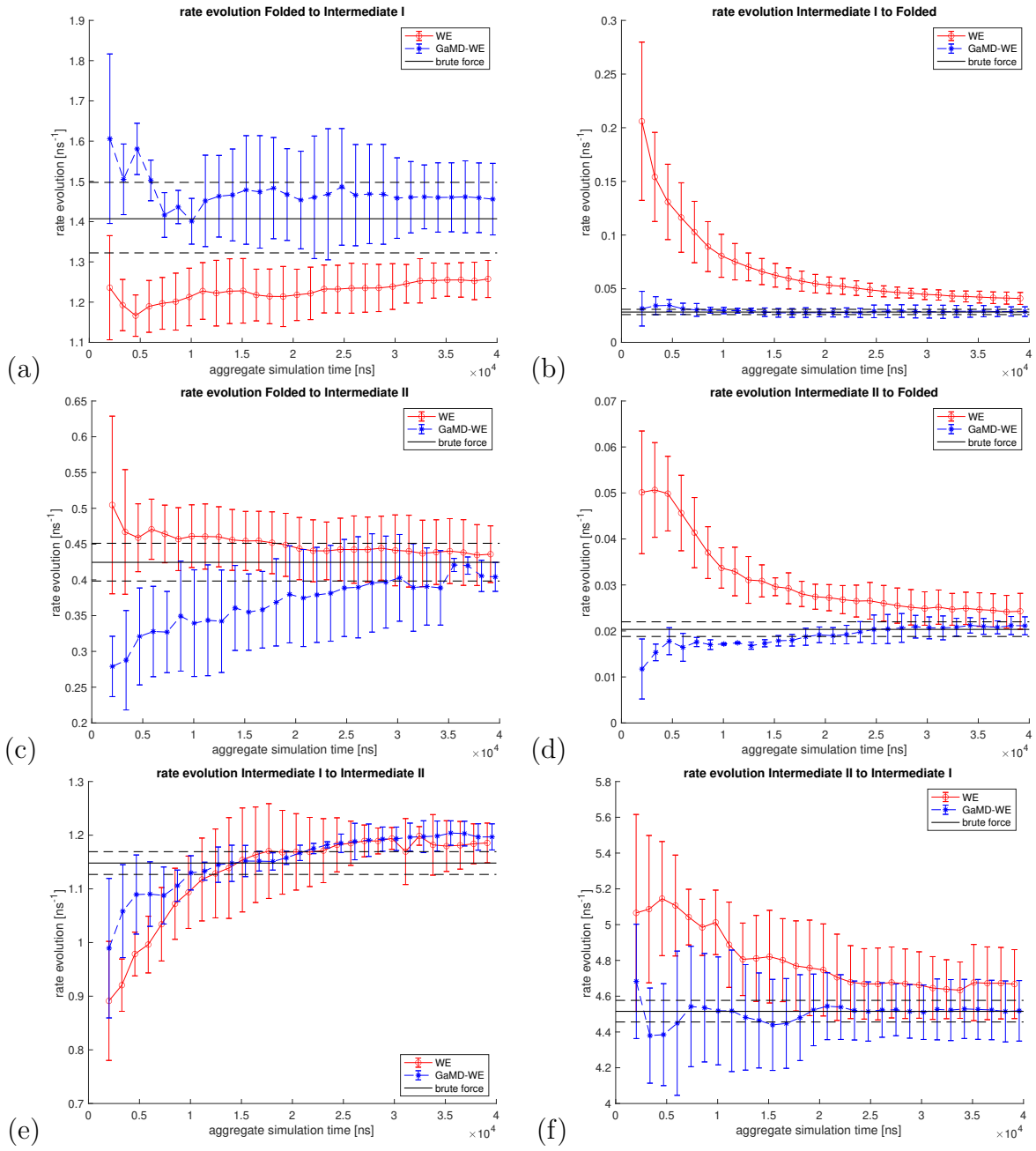

Figure 5: Evolution of rate constants over aggregate simulation time for WE (in red) and GaMD-WE (in blue). The reference brute force values are in black. (a) and (b) show the rate constants between the folded region and the intermediate I region. (c) and (d) show the rate constants between the folded region and the intermediate II region. (e) and (f) show the rate constants between the intermediate I region and the intermediate II region.

3.3 Bovine pancreatic trypsin inhibitor

As a final test, we ran a GaMD simulation and a WE simulation of bovine pancreatic trypsin inhibitor (BPTI), an 892-atom system with 58 residues (PDB: 5PTI). This was to test whether GaMD will be more effective than WE at covering the free energy landscape of a bigger protein system than alanine dipeptide or chignolin. TIP4P-Ew water model[93] was used to solvate the system explicitly. Both simulations were run for 500 ns. Simulation time, τ for WE was set to 40 ps, and points were sampled every 2 ps to match GaMD's sampling frequency. Target number of walkers per macrostate n_w was set to 4. CVs were set to be the dihedral angles χ_1-C14 and χ_1-C38 associated with the disulfide bond formed between cysteine 14 and cysteine 38.[94,95] Macrostates were evenly spaced in intervals of 10° for both (ranging from -180° to 180°).

Figures 6a and 6b show the free energy landscape ($-k_BT\ln P$, where P denotes probability) of BPTI after one 500 ns run of GaMD and WE, respectively. The lowest energy state was set to be zero for each of the free energy landscapes. In particular, the GaMD run with the upper bound of the dual boost potential yielded the maximum number of initial structures on average as compared to the other five GaMD potential settings (see Supplementary Information). Maclaurin expansion to the tenth order was used for GaMD reweighting since using cumulant expansion to the second order is limited for small proteins with 40 residues or less.[1] Figure 6a shows a free energy landscape similar to the one obtained from accelerated molecular dynamics (aMD), which was also obtained using a dual boost potential and Maclaurin expansion to the tenth order for reweighting.[95] Slight differences between the two free energy landscapes may be from using different force field parameters: aMD used the modified Amber ff99SB-ILDN force field,[96,97] which removed modifications to leucine, aspartic acid, and asparagine to mimic the Anton simulation of BPTI,[98] and GaMD used the Amber ff14SB force field.[90]

Metastable states of interest, including the major state M and two minor or excited states m_{C14} and m_{C38},[99] are marked in Figure 6a. M region was defined to be $-120° < \chi_1 - \text{C14} <$

$0°$, $0° < \chi_1 - \text{C38} < 120°$, $0° < \chi_3 < 180°$, m_{C14} was defined to be $0° < \chi_1 - \text{C14} < 120°$, $0° < \chi_1 - \text{C38} < 120°$, $-180° < \chi_3 < 0°$, and m_{C38} was defined to be $-120° < \chi_1 - \text{C14} < 0°$, $-120° < \chi_1 - \text{C38} < 0°$, $-180° < \chi_3 < 0°$ as in the BPTI aMD reference.[94,95] Dihedral angle χ_3 is associated with the disulfide bond formed between cysteine 14 and cysteine 38. It is clear that GaMD is more effective at exploring other metastable states present in BPTI including m_{C14} as compared to WE. Even after extending the WE simulation for 2 μs (total simulation time: 2.5 μs), WE is still not able to sample m_{C14} as seen in Figure 6c. This highlights the power of GaMD being able to sample more of the configuration space than WE. GaMD can sample orthogonal modes to the chosen CVs $\chi_1-\text{C14}$ and $\chi_1-\text{C38}$ since it is a CV free enhanced sampling method. In contrast, WE mainly samples along the chosen CVs and can encounter difficulties in sampling regions when there are orthogonal modes present to the chosen CVs. Although rate constants between these metastable states were not measured, it is expected that GaMD-WE will sample them significantly faster than conventional WE.

4 Discussion

Three examples mentioned in the previous sections highlight how GaMD-WE can be more powerful than either GaMD or WE by itself. On the other hand, this hybrid method also reveals both methods' advantages and disadvantages. GaMD is more effective at sampling the configuration space than WE by being a CV-free method. By adding boost potentials to "fill" the energy wells in a CV-free manner, GaMD can sample the configuration space more evenly across different modes in the system. On the other hand, WE is mainly limited to efficiently sampling along the chosen CVs. This is not problematic if the chosen CVs sufficiently describe the dynamics of the system, but in most cases, it is difficult to know the best CVs *a priori*. In such cases, WE can be slow at sampling the configuration space with the orthogonal modes present. For alanine dipeptide and chignolin, chosen CVs have

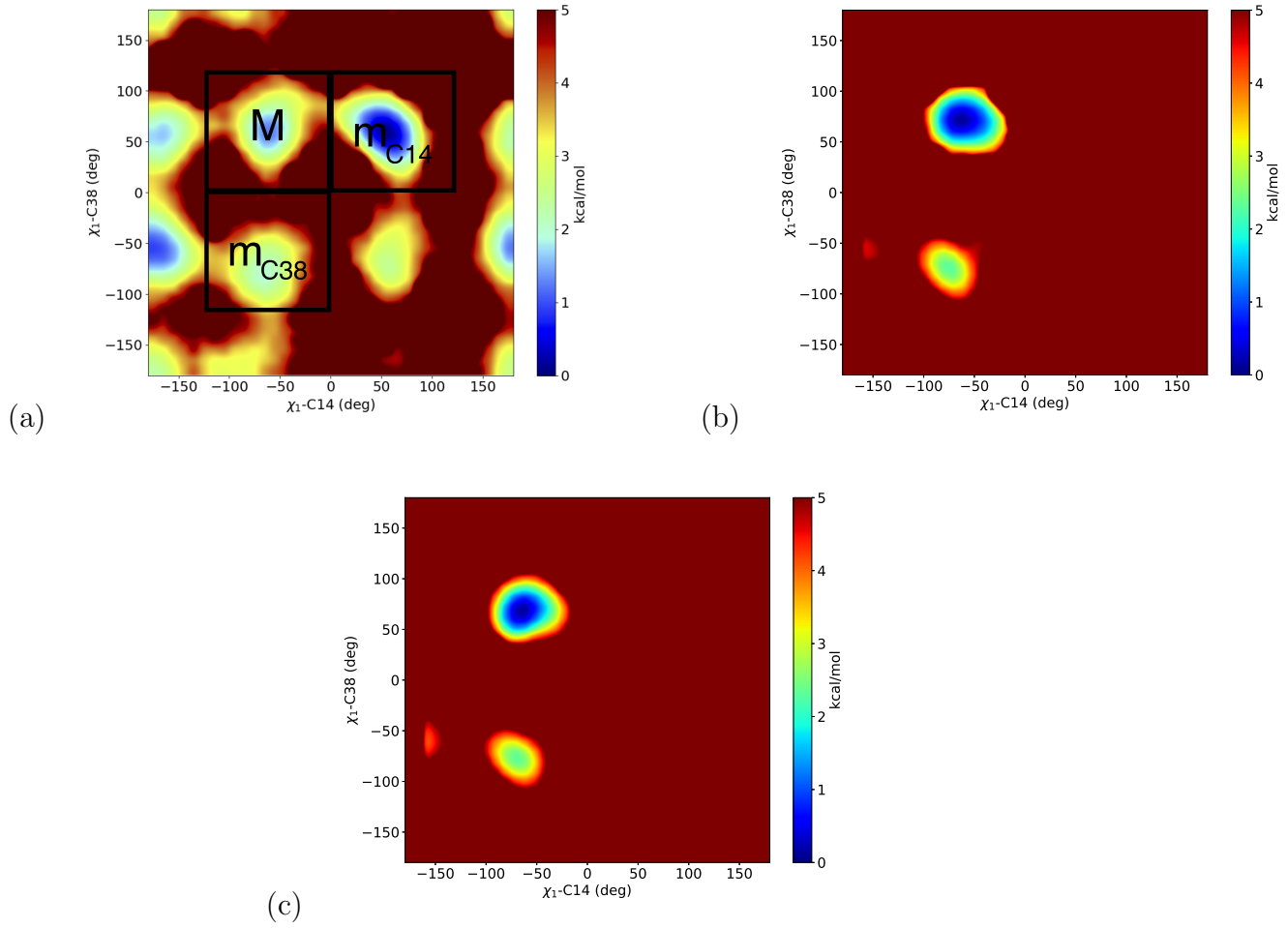

Figure 6: Free energy landscape ($-k_B T \ln P$, where P denotes probability) of BPTI after (a) one 500 ns run of GaMD (with upper bound of dual boost potential) with metastable states of interest M, m_{C14}, and m_{C38} marked, (b) one 500 ns run of WE, and (c) extending WE run for 2 μs (total simulation time: 2.5 μs), respectively. The lowest energy state was set to be zero for each of the free energy landscapes.

been commonly used in existing literatures.[1,51,87] They are small enough systems for both GaMD and WE to sufficiently sample well. But for BPTI, the dihedral angles χ_1-C14 and χ_1-C38 are not commonly used CVs and have shown to be insufficient for WE to sample as effectively as GaMD. BPTI is also a much bigger system than alanine dipeptide or chignolin. In this case, principal component analysis (PCA) vectors have been commonly used instead as CVs for BPTI.[95,98,100]

Another limitation of WE is that it cannot have CVs such as PCA vectors, which can only reliably be obtained from a long simulation. GaMD, Markov state models (MSMs), and other methods that are post-processed, constructed, and analyzed after a long simulation is run can have PCA vectors, time-structure based independent component analysis (tICA) vectors, and other dimensionality reduction vectors to describe the system.[60,101] Nonetheless, WE can have non-differentiable CVs such as the number of hydrogen bonds, which can be helpful for many systems. In contrast, other methods such as metadynamics and adaptive biasing force (ABF) need differentiable CVs. Moreover, WE does not add any statistical bias to the system and is exact regardless of the parameters,[102] so it can reliably obtain the actual kinetics of the system. Since a long simulation is typically needed to get reasonable estimates of the kinetics, researchers have recently developed methods for WE to estimate the actual kinetics faster.[52,103,104] If GaMD-WE is combined with these current methods, more improvements will be seen in obtaining thermodynamic and kinetic properties.

5 Conclusion

We have combined two well-established enhanced sampling methods, GaMD and WE, into a hybrid method GaMD-WE to create a more powerful enhanced sampling method for MD simulations. GaMD is used to sample the free energy landscape initially, and WE is used to further sample the free energy landscape and ascertain rate constants between two states of interest in the system of interest. We have shown how the hybrid method performs

better than conventional WE in sampling thermodynamic and kinetic properties for three systems, and its performance significantly improves as the system size grows. For future directions, we plan to fully integrate the hybrid method with a WE simulation toolkit such as WESTPA and possibly combine it with other WE enhancing algorithms to create state-of-the-art enhanced sampling methods. The GaMD-WE package is available at `https://github.com/anandojha/gamd_we` and the documentation is available at `https://gamd-we.readthedocs.io/en/latest/`.

Acknowledgement

S.A. acknowledges support from NIH GM31749 and the University of California San Diego. All simulations were done at the Triton Shared Computing Cluster (TSCC), San Diego Supercomputing Center (SDSC).

Supporting Information Available

Supporting information includes results from the other GaMD runs for alanine dipeptide, chignolin, and BPTI, which were used to pick the best GaMD run to start the GaMD-WE simulations for alanine dipeptide and chignolin.

References

(1) Miao, Y.; Feher, V. A.; McCammon, J. A. Gaussian accelerated molecular dynamics: Unconstrained enhanced sampling and free energy calculation. *Journal of Chemical Theory and Computation* **2015**, *11*, 3584–3595.

(2) Pang, Y. T.; Miao, Y.; Wang, Y.; McCammon, J. A. Gaussian accelerated molecular dynamics in NAMD. *Journal of Chemical Theory and Computation* **2017**, *13*, 9–19.

(3) Miao, Y.; McCammon, J. A. *Annual Reports in Computational Chemistry*; Elsevier, 2017; Vol. 13; pp 231–278.

(4) Wang, J.; Arantes, P. R.; Bhattarai, A.; Hsu, R. V.; Pawnikar, S.; Huang, Y.-m. M.; Palermo, G.; Miao, Y. Gaussian accelerated molecular dynamics: Principles and applications. *Wiley Interdisciplinary Reviews: Computational Molecular Science* **2021**, e1521.

(5) Barducci, A.; Bonomi, M.; Parrinello, M. Metadynamics. *Wiley Interdisciplinary Reviews: Computational Molecular Science* **2011**, *1*, 826–843.

(6) Laio, A.; Rodriguez-Fortea, A.; Gervasio, F. L.; Ceccarelli, M.; Parrinello, M. Assessing the accuracy of metadynamics. *The Journal of Physical Chemistry B* **2005**, *109*, 6714–6721.

(7) Bussi, G.; Laio, A.; Parrinello, M. Equilibrium free energies from nonequilibrium metadynamics. *Physical Review Letters* **2006**, *96*, 090601.

(8) Barducci, A.; Bussi, G.; Parrinello, M. Well-tempered metadynamics: a smoothly converging and tunable free-energy method. *Physical Review Letters* **2008**, *100*, 020603.

(9) Laio, A.; Gervasio, F. L. Metadynamics: a method to simulate rare events and reconstruct the free energy in biophysics, chemistry and material science. *Reports on Progress in Physics* **2008**, *71*, 126601.

(10) Torrie, G. M.; Valleau, J. P. Nonphysical sampling distributions in Monte Carlo free-energy estimation: Umbrella sampling. *Journal of Computational Physics* **1977**, *23*, 187–199.

(11) Kästner, J. Umbrella sampling. *Wiley Interdisciplinary Reviews: Computational Molecular Science* **2011**, *1*, 932–942.

(12) Virnau, P.; Müller, M. Calculation of free energy through successive umbrella sampling. *The Journal of Chemical Physics* **2004**, *120*, 10925–10930.

(13) Warmflash, A.; Bhimalapuram, P.; Dinner, A. R. Umbrella sampling for nonequilibrium processes. *The Journal of Chemical Physics* **2007**, *127*, 114109.

(14) Darve, E.; Rodríguez-Gómez, D.; Pohorille, A. Adaptive biasing force method for scalar and vector free energy calculations. *The Journal of Chemical Physics* **2008**, *128*, 144120.

(15) Comer, J.; Gumbart, J. C.; Hénin, J.; Lelièvre, T.; Pohorille, A.; Chipot, C. The adaptive biasing force method: Everything you always wanted to know but were afraid to ask. *The Journal of Physical Chemistry B* **2015**, *119*, 1129–1151.

(16) Darve, E.; Pohorille, A. Calculating free energies using average force. *The Journal of Chemical Physics* **2001**, *115*, 9169–9183.

(17) Chipot, C.; Pohorille, A. Free energy calculations. *Springer Series in Chemical Physics* **2007**, *86*, 159–184.

(18) Lelièvre, T.; Rousset, M.; Stoltz, G. Long-time convergence of an adaptive biasing force method. *Nonlinearity* **2008**, *21*, 1155.

(19) Sugita, Y.; Okamoto, Y. Replica-exchange molecular dynamics method for protein folding. *Chemical Physics Letters* **1999**, *314*, 141–151.

(20) Sindhikara, D.; Meng, Y.; Roitberg, A. E. Exchange frequency in replica exchange molecular dynamics. *The Journal of Chemical Physics* **2008**, *128*, 01B609.

(21) Zhang, W.; Wu, C.; Duan, Y. Convergence of replica exchange molecular dynamics. *The Journal of Chemical Physics* **2005**, *123*, 154105.

(22) Sindhikara, D. J.; Emerson, D. J.; Roitberg, A. E. Exchange often and properly in replica exchange molecular dynamics. *Journal of Chemical Theory and Computation* **2010**, *6*, 2804–2808.

(23) Rosta, E.; Hummer, G. Error and efficiency of replica exchange molecular dynamics simulations. *The Journal of Chemical Physics* **2009**, *131*, 10B615.

(24) Miao, Y. Acceleration of biomolecular kinetics in Gaussian accelerated molecular dynamics. *The Journal of Chemical Physics* **2018**, *149*, 072308.

(25) Stelzl, L. S.; Hummer, G. Kinetics from replica exchange molecular dynamics simulations. *Journal of Chemical Theory and Computation* **2017**, *13*, 3927–3935.

(26) Buchete, N.-V.; Hummer, G. Peptide folding kinetics from replica exchange molecular dynamics. *Physical Review E* **2008**, *77*, 030902.

(27) Tiwary, P.; Parrinello, M. From metadynamics to dynamics. *Physical Review Letters* **2013**, *111*, 230602.

(28) Faradjian, A. K.; Elber, R. Computing time scales from reaction coordinates by milestoning. *The Journal of Chemical Physics* **2004**, *120*, 10880–10889.

(29) Vanden-Eijnden, E.; Venturoli, M.; Ciccotti, G.; Elber, R. On the assumptions underlying milestoning. *The Journal of Chemical Physics* **2008**, *129*, 174102.

(30) Bello-Rivas, J. M.; Elber, R. Exact milestoning. *The Journal of Chemical Physics* **2015**, *142*, 03B602_1.

(31) Májek, P.; Elber, R. Milestoning without a reaction coordinate. *Journal of Chemical Theory and Computation* **2010**, *6*, 1805–1817.

(32) Vanden-Eijnden, E.; Venturoli, M. Markovian milestoning with Voronoi tessellations. *The Journal of Chemical Physics* **2009**, *130*, 194101.

(33) Allen, R. J.; Valeriani, C.; Ten Wolde, P. R. Forward flux sampling for rare event simulations. *Journal of Physics: Condensed Matter* **2009**, *21*, 463102.

(34) Allen, R. J.; Frenkel, D.; Ten Wolde, P. R. Forward flux sampling-type schemes for simulating rare events: Efficiency analysis. *The Journal of Chemical Physics* **2006**, *124*, 194111.

(35) Valeriani, C.; Allen, R. J.; Morelli, M. J.; Frenkel, D.; Rein ten Wolde, P. Computing stationary distributions in equilibrium and nonequilibrium systems with forward flux sampling. *The Journal of Chemical Physics* **2007**, *127*, 114109.

(36) Hussain, S.; Haji-Akbari, A. Studying rare events using forward-flux sampling: Recent breakthroughs and future outlook. *The Journal of Chemical Physics* **2020**, *152*, 060901.

(37) Van Erp, T. S.; Bolhuis, P. G. Elaborating transition interface sampling methods. *Journal of Computational Physics* **2005**, *205*, 157–181.

(38) Moroni, D.; van Erp, T. S.; Bolhuis, P. G. Investigating rare events by transition interface sampling. *Physica A: Statistical Mechanics and its Applications* **2004**, *340*, 395–401.

(39) Borrero, E. E.; Weinwurm, M.; Dellago, C. Optimizing transition interface sampling simulations. *The Journal of Chemical Physics* **2011**, *134*, 244118.

(40) Du, W.-N.; Marino, K. A.; Bolhuis, P. G. Multiple state transition interface sampling of alanine dipeptide in explicit solvent. *The Journal of Chemical Physics* **2011**, *135*, 10B609.

(41) Bowman, G. R.; Pande, V. S.; Noé, F. *An introduction to Markov state models and their application to long timescale molecular simulation*; Springer Science & Business Media, 2013; Vol. 797.

(42) Chodera, J. D.; Noé, F. Markov state models of biomolecular conformational dynamics. *Current Opinion in Structural Biology* **2014**, *25*, 135–144.

(43) Husic, B. E.; Pande, V. S. Markov state models: From an art to a science. *Journal of the American Chemical Society* **2018**, *140*, 2386–2396.

(44) Chodera, J. D.; Singhal, N.; Pande, V. S.; Dill, K. A.; Swope, W. C. Automatic discovery of metastable states for the construction of Markov models of macromolecular conformational dynamics. *The Journal of Chemical Physics* **2007**, *126*, 04B616.

(45) Pande, V. S.; Beauchamp, K.; Bowman, G. R. Everything you wanted to know about Markov State Models but were afraid to ask. *Methods* **2010**, *52*, 99–105.

(46) Shukla, D.; Hernández, C. X.; Weber, J. K.; Pande, V. S. Markov state models provide insights into dynamic modulation of protein function. *Accounts of Chemical Research* **2015**, *48*, 414–422.

(47) Bowman, G. R.; Beauchamp, K. A.; Boxer, G.; Pande, V. S. Progress and challenges in the automated construction of Markov state models for full protein systems. *The Journal of Chemical Physics* **2009**, *131*, 124101.

(48) Bowman, G. R.; Huang, X.; Pande, V. S. Using generalized ensemble simulations and Markov state models to identify conformational states. *Methods* **2009**, *49*, 197–201.

(49) Huber, G. A.; Kim, S. Weighted-ensemble Brownian dynamics simulations for protein association reactions. *Biophysical Journal* **1996**, *70*, 97–110.

(50) Zuckerman, D. M.; Chong, L. T. Weighted ensemble simulation: review of methodology, applications, and software. *Annual Review of Biophysics* **2017**, *46*, 43–57.

(51) Zhang, B. W.; Jasnow, D.; Zuckerman, D. M. The "weighted ensemble" path sampling method is statistically exact for a broad class of stochastic processes and binning procedures. *The Journal of Chemical Physics* **2010**, *132*, 054107.

(52) Copperman, J.; Zuckerman, D. M. Accelerated Estimation of Long-Timescale Kinetics from Weighted Ensemble Simulation via Non-Markovian "Microbin" Analysis. *Journal of Chemical Theory and Computation* **2020**, *16*, 6763–6775.

(53) Bhatt, D.; Zhang, B. W.; Zuckerman, D. M. Steady-state simulations using weighted ensemble path sampling. *The Journal of Chemical Physics* **2010**, *133*, 014110.

(54) Dickson, A.; Brooks III, C. L. WExplore: hierarchical exploration of high-dimensional spaces using the weighted ensemble algorithm. *The Journal of Physical Chemistry B* **2014**, *118*, 3532–3542.

(55) Donyapour, N.; Roussey, N. M.; Dickson, A. REVO: Resampling of ensembles by variation optimization. *The Journal of Chemical Physics* **2019**, *150*, 244112.

(56) Ahn, S.-H.; Grate, J. W.; Darve, E. F. Efficiently sampling conformations and pathways using the concurrent adaptive sampling (CAS) algorithm. *The Journal of Chemical Physics* **2017**, *147*, 074115.

(57) Abdul-Wahid, B.; Feng, H.; Rajan, D.; Costaouec, R.; Darve, E.; Thain, D.; Izaguirre, J. A. AWE-WQ: fast-forwarding molecular dynamics using the accelerated weighted ensemble. *Journal of Chemical Information and Modeling* **2014**, *54*, 3033–3043.

(58) Yu, L.; Rajan, D.; Feng, H.; Darve, E.; Thain, D.; Izaguirre, J. A., et al. Folding Proteins at 500 ns/hour with Work Queue. 2012 IEEE 8th International Conference on E-Science. 2012; pp 1–8.

(59) Costaouec, R.; Feng, H.; Izaguirre, J.; Darve, E. Analysis of the accelerated weighted ensemble methodology. Conference Publications. 2013; p 171.

(60) Schwantes, C. R.; Pande, V. S. Improvements in Markov state model construction

reveal many non-native interactions in the folding of NTL9. *Journal of chemical theory and computation* **2013**, *9*, 2000–2009.

(61) Lane, T. J.; Bowman, G. R.; Beauchamp, K.; Voelz, V. A.; Pande, V. S. Markov state model reveals folding and functional dynamics in ultra-long MD trajectories. *Journal of the American Chemical Society* **2011**, *133*, 18413–18419.

(62) Weber, J. K.; Pande, V. S. Characterization and rapid sampling of protein folding Markov state model topologies. *Journal of Chemical Theory and Computation* **2011**, *7*, 3405–3411.

(63) Rosta, E.; Hummer, G. Free energies from dynamic weighted histogram analysis using unbiased Markov state model. *Journal of Chemical Theory and Computation* **2015**, *11*, 276–285.

(64) Zimmerman, M. I.; Bowman, G. R. FAST conformational searches by balancing exploration/exploitation trade-offs. *Journal of Chemical Theory and Computation* **2015**, *11*, 5747–5757.

(65) Zimmerman, M. I.; Porter, J. R.; Ward, M. D.; Singh, S.; Vithani, N.; Meller, A.; Mallimadugula, U. L.; Kuhn, C. E.; Borowsky, J. H.; Wiewiora, R. P., et al. SARS-CoV-2 simulations go exascale to predict dramatic spike opening and cryptic pockets across the proteome. *Nature Chemistry* **2021**, 1–9.

(66) Adelman, J. L.; Grabe, M. Simulating current–voltage relationships for a narrow ion channel using the weighted ensemble method. *Journal of Chemical Theory and Computation* **2015**, *11*, 1907–1918.

(67) Adhikari, U.; Mostofian, B.; Copperman, J.; Subramanian, S. R.; Petersen, A. A.; Zuckerman, D. M. Computational estimation of microsecond to second atomistic folding times. *Journal of the American Chemical Society* **2019**, *141*, 6519–6526.

(68) Saglam, A. S.; Chong, L. T. Protein–protein binding pathways and calculations of rate constants using fully-continuous, explicit-solvent simulations. *Chemical Science* **2019**, *10*, 2360–2372.

(69) Dixon, T.; Lotz, S. D.; Dickson, A. Predicting ligand binding affinity using on-and off-rates for the SAMPL6 SAMPLing challenge. *Journal of Computer-Aided Molecular Design* **2018**, *32*, 1001–1012.

(70) Lotz, S. D.; Dickson, A. Unbiased molecular dynamics of 11 min timescale drug unbinding reveals transition state stabilizing interactions. *Journal of the American Chemical Society* **2018**, *140*, 618–628.

(71) Sztain, T.; Ahn, S.-H.; Bogetti, A. T.; Casalino, L.; Goldsmith, J. A.; McCool, R. S.; Kearns, F. L.; McCammon, J. A.; McLellan, J. S.; Chong, L. T., et al. A glycan gate controls opening of the SARS-CoV-2 spike protein. *bioRxiv* **2021**,

(72) Ahn, S.-H.; Grate, J. W.; Darve, E. F. Investigating the role of non-covalent interactions in conformation and assembly of triazine-based sequence-defined polymers. *The Journal of Chemical Physics* **2018**, *149*, 072330.

(73) Ahn, S.-H.; Grate, J. W. Foldamer Architectures of Triazine-Based Sequence-Defined Polymers Investigated with Molecular Dynamics Simulations and Enhanced Sampling Methods. *The Journal of Physical Chemistry B* **2019**, *123*, 9364–9377.

(74) Ahn, S.-H.; Jagger, B. R.; Amaro, R. E. Ranking of ligand binding kinetics using a weighted ensemble approach and comparison with a multiscale milestoning approach. *Journal of Chemical Information and Modeling* **2020**, *60*, 5340–5352.

(75) Barros, E. P.; Demir, Ö.; Soto, J.; Cocco, M. J.; Amaro, R. E. Markov state models and NMR uncover an overlooked allosteric loop in p53. *Chemical Science* **2021**, *12*, 1891–1900.

(76) Durrant, J. D.; Kochanek, S. E.; Casalino, L.; Ieong, P. U.; Dommer, A. C.; Amaro, R. E. Mesoscale all-atom influenza virus simulations suggest new substrate binding mechanism. *ACS Central Science* **2020**, *6*, 189–196.

(77) Taylor, B. C.; Lee, C. T.; Amaro, R. E. Structural basis for ligand modulation of the CCR2 conformational landscape. *Proceedings of the National Academy of Sciences* **2019**, *116*, 8131–8136.

(78) Huang, Y.-m. M.; McCammon, J. A.; Miao, Y. Replica exchange Gaussian accelerated molecular dynamics: Improved enhanced sampling and free energy calculation. *Journal of Chemical Theory and Computation* **2018**, *14*, 1853–1864.

(79) Oshima, H.; Re, S.; Sugita, Y. Replica-exchange umbrella sampling combined with gaussian accelerated molecular dynamics for free-energy calculation of biomolecules. *Journal of Chemical Theory and Computation* **2019**, *15*, 5199–5208.

(80) Chen, H.; Fu, H.; Chipot, C.; Shao, X.; Cai, W. Overcoming Free-Energy Barriers with a Seamless Combination of a Biasing Force and a Collective Variable-Independent Boost Potential. *Journal of Chemical Theory and Computation* **2021**,

(81) Trapl, D.; Horvacanin, I.; Mareska, V.; Ozcelik, F.; Unal, G.; Spiwok, V. Anncolvar: approximation of complex collective variables by artificial neural networks for analysis and biasing of molecular simulations. *Frontiers in Molecular Biosciences* **2019**, *6*, 25.

(82) Fiorin, G.; Klein, M. L.; Hénin, J. Using collective variables to drive molecular dynamics simulations. *Molecular Physics* **2013**, *111*, 3345–3362.

(83) Sittel, F.; Stock, G. Perspective: Identification of collective variables and metastable states of protein dynamics. *The Journal of Chemical Physics* **2018**, *149*, 150901.

(84) Case, D. A.; Belfon, K.; Ben-Shalom, I.; Brozell, S. R.; Cerutti, D.; Cheatham, T.; Cruzeiro, V. W. D.; Darden, T.; Duke, R. E.; Giambasu, G., et al. Amber 2020. **2020**,

(85) Phillips, J. C.; Hardy, D. J.; Maia, J. D.; Stone, J. E.; Ribeiro, J. V.; Bernardi, R. C.; Buch, R.; Fiorin, G.; Hénin, J.; Jiang, W., et al. Scalable molecular dynamics on CPU and GPU architectures with NAMD. *The Journal of Chemical Physics* **2020**, *153*, 044130.

(86) Zwier, M. C.; Adelman, J. L.; Kaus, J. W.; Pratt, A. J.; Wong, K. F.; Rego, N. B.; Suárez, E.; Lettieri, S.; Wang, D. W.; Grabe, M., et al. WESTPA: An interoperable, highly scalable software package for weighted ensemble simulation and analysis. *Journal of Chemical Theory and Computation* **2015**, *11*, 800–809.

(87) Bogetti, A. T.; Mostofian, B.; Dickson, A.; Pratt, A.; Saglam, A. S.; Harrison, P. O.; Adelman, J. L.; Dudek, M.; Torrillo, P. A.; DeGrave, A. J., et al. A suite of tutorials for the WESTPA rare-events sampling software [Article v1. 0]. *Living Journal of Computational Molecular Science* **2019**, *1*.

(88) Pratt, A.; Suárez, E.; Zuckerman, D. M.; Chong, L. T. Extensive Evaluation of Weighted Ensemble Strategies for Calculating Rate Constants and Binding Affinities of Molecular Association/Dissociation Processes. *bioRxiv* **2019**, 671172.

(89) Eastman, P.; Swails, J.; Chodera, J. D.; McGibbon, R. T.; Zhao, Y.; Beauchamp, K. A.; Wang, L.-P.; Simmonett, A. C.; Harrigan, M. P.; Stern, C. D., et al. OpenMM 7: Rapid development of high performance algorithms for molecular dynamics. *PLoS Computational Biology* **2017**, *13*, e1005659.

(90) Maier, J. A.; Martinez, C.; Kasavajhala, K.; Wickstrom, L.; Hauser, K. E.; Simmerling, C. ff14SB: improving the accuracy of protein side chain and backbone parameters from ff99SB. *Journal of Chemical Theory and Computation* **2015**, *11*, 3696–3713.

(91) MacKerell Jr, A. D.; Bashford, D.; Bellott, M.; Dunbrack Jr, R. L.; Evanseck, J. D.; Field, M. J.; Fischer, S.; Gao, J.; Guo, H.; Ha, S., et al. All-atom empirical potential

for molecular modeling and dynamics studies of proteins. *The Journal of Physical Chemistry B* **1998**, *102*, 3586–3616.

(92) Onufriev, A.; Bashford, D.; Case, D. A. Modification of the generalized Born model suitable for macromolecules. *The Journal of Physical Chemistry B* **2000**, *104*, 3712–3720.

(93) Horn, H. W.; Swope, W. C.; Pitera, J. W.; Madura, J. D.; Dick, T. J.; Hura, G. L.; Head-Gordon, T. Development of an improved four-site water model for biomolecular simulations: TIP4P-Ew. *The Journal of Chemical Physics* **2004**, *120*, 9665–9678.

(94) Xue, Y.; Ward, J. M.; Yuwen, T.; Podkorytov, I. S.; Skrynnikov, N. R. Microsecond time-scale conformational exchange in proteins: using long molecular dynamics trajectory to simulate NMR relaxation dispersion data. *Journal of the American Chemical Society* **2012**, *134*, 2555–2562.

(95) Pierce, L. C.; Salomon-Ferrer, R.; Augusto F. de Oliveira, C.; McCammon, J. A.; Walker, R. C. Routine access to millisecond time scale events with accelerated molecular dynamics. *Journal of Chemical Theory and Computation* **2012**, *8*, 2997–3002.

(96) Hornak, V.; Abel, R.; Okur, A.; Strockbine, B.; Roitberg, A.; Simmerling, C. Comparison of multiple Amber force fields and development of improved protein backbone parameters. *Proteins: Structure, Function, and Bioinformatics* **2006**, *65*, 712–725.

(97) Lindorff-Larsen, K.; Piana, S.; Palmo, K.; Maragakis, P.; Klepeis, J. L.; Dror, R. O.; Shaw, D. E. Improved side-chain torsion potentials for the Amber ff99SB protein force field. *Proteins: Structure, Function, and Bioinformatics* **2010**, *78*, 1950–1958.

(98) Shaw, D. E.; Maragakis, P.; Lindorff-Larsen, K.; Piana, S.; Dror, R. O.; Eastwood, M. P.; Bank, J. A.; Jumper, J. M.; Salmon, J. K.; Shan, Y., et al. Atomic-level characterization of the structural dynamics of proteins. *Science* **2010**, *330*, 341–346.

(99) Grey, M. J.; Wang, C.; Palmer, A. G. Disulfide bond isomerization in basic pancreatic trypsin inhibitor: multisite chemical exchange quantified by CPMG relaxation dispersion and chemical shift modeling. *Journal of the American Chemical Society* **2003**, *125*, 14324–14335.

(100) Ernst, M.; Sittel, F.; Stock, G. Contact-and distance-based principal component analysis of protein dynamics. *The Journal of Chemical Physics* **2015**, *143*, 12B640_1.

(101) Pérez-Hernández, G.; Paul, F.; Giorgino, T.; De Fabritiis, G.; Noé, F. Identification of slow molecular order parameters for Markov model construction. *The Journal of Chemical Physics* **2013**, *139*, 07B604_1.

(102) Aristoff, D.; Zuckerman, D. M. Optimizing weighted ensemble sampling of steady states. *Multiscale Modeling & Simulation* **2020**, *18*, 646–673.

(103) DeGrave, A. J.; Bogetti, A. T.; Chong, L. T. The RED scheme: Rate-constant estimation from pre-steady state weighted ensemble simulations. *The Journal of Chemical Physics* **2021**, *154*, 114111.

(104) Torrillo, P. A.; Bogetti, A. T.; Chong, L. T. A minimal, adaptive binning scheme for weighted ensemble simulations. *The Journal of Physical Chemistry A* **2021**, *125*, 1642–1649.

Graphical TOC Entry